The odd weight of granular packings: Effect of grain geometry

Iker Zamorano Vega*
Facultat de Física, Universitat de Barcelona, Diagonal 645, 08028 Barcelona, Spain

Advisors: Ramon Planet and Alberto Fernandez-Nieves
(Dated: July 2022)

Granular materials are collections of solid grains that exhibit unusual mechanical properties. In 1895, the engineer Janssen found that when filling a silo with corn grains, the pressure at the bottom of the column rather than increasing linearly with the added mass showed a saturation [5]. Recently, this experiment has been repeated using spherical grains on narrow containers, where the pressure at the bottom exhibits an overshoot region, meaning that the apparent mass is larger than the added mass before saturating [14]. In this work we revisit those experiments now using two different grain geometries, being oblate and prolate grains, with the aim of studying its behaviour on narrow containers and if the *reversed* Janssen effect is still observed using these grain geometries. It is found that for tubes with large diameters both, oblate and prolate particles, exhibit the saturation of mass for large added mass, the qualitative response described by Janssen. As the diameter of the tube decreases, the overshoot regions gain more importance at intermediate added masses. However, the model introduced in [14] for spheres does not describe properly the results obtained. Now, the magnitude of the overshoot decays faster with the increasing size of the container. Furthermore, it is observed that the average packing fraction of the granular columns does increase until saturating, which may be related to the saturation of the pressure on the granular column.

I. INTRODUCTION

From dunes of deserts to the bowl of rice we eat for lunch, passing through powders used to make cement, grains are one of the most common kind of materials in our daily life. There is a wide range of applications for such materials, as in the alimentary industry, where they deal with different cereals and legumes or the pharmaceutical industry, where they use powders as the main source of developing their products, among others. Despite its ubiquitous presence in many technological areas, granular matter lacks of a general description due to the intrinsic complexity of the collective behaviour of grains. Granular materials are solid particles with length-scales $d > 1\,\mu$m such that thermal agitation and Brownian motion can be neglected [1, 2]. From a thermodynamic perspective, these systems are out of equilibrium. The different configurations granular media can adopt correspond to metastable states,meaning that the system will remain in this state unless there are external perturbations that allow the granular media adopt a new state [1–3].

The collective behavior of granular media do not consist on the sum of each individual grain. For dry and cohesionless grains, there are no attractive forces playing an important role, so that frictional forces and body forces, such as gravity, are the relevant forces. Furthermore, the state of the system depends on protocol [11].

Its complex behavior result from the presence of the so-called "force chains" [3]. These are fractal-like structures consisting on strings of rigid particles that are aligned and in co-linear contact. When shearing a granular material, force-chains will develop to oppose the applied deformation. However, when applying a deformation whose direction is not the chain's principal axis the structure will not be able to sustain and will behave as a brittle material. During this process the force-chains break and rearrange [4].

As storing and transporting grains is a common thing for industries, several studies of the static distribution of granular media have been performed along the years, focusing mainly on the relations between stress and strain. One of the most famous experiments involving granular media is the one performed by Janssen [5, 6] and has been reproduced under different conditions [9, 10]. It dates back to 1895 when the German engineer tried to figure out the reason why the silos used to store the corn break by the sides at a given height when filled with grains, instead of doing it at the bottom. To do so, he developed an experiment which consisted on filling up a cylindrical container with corn up to a given height and then measure the pressure exerted at the bottom solely by the granular column, see Fig.1 a). Once the measure was done, more grains were inserted into the container, repeating this process several times. The results obtained for the pressure at the bottom of the column of hegiht h, $P(h)$, was that it increased with the added mass up to a point where it saturates rather than keep on increasing when adding more grains, as it would do a fluid, $P(h) = \rho g h$ (where ρ is the mean density of the fluid and g is the gravitational acceleration $g = 9.8\,\mathrm{m/s^2}$), see Fig.1 b). This was an indicator that frictional forces inside the granular column play a significant role. Friction forces compensates the weight of the added grains thanks to the presence of force-chains, thus preventing the pressure at the bottom from increase.

* izamorve7@alumnes.ub.edu

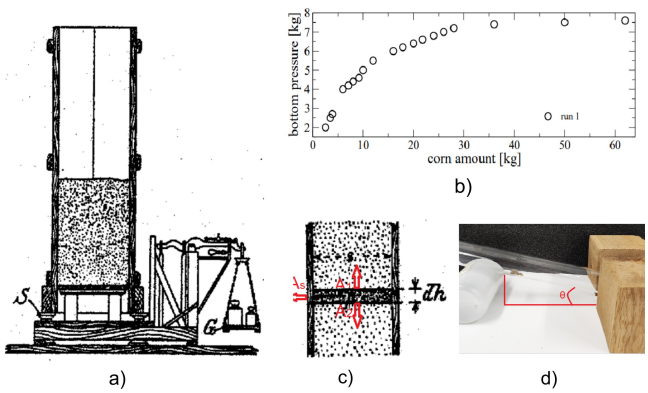

FIG. 1. a): Original Janssen experimental set-up for measuring the bottom pressure. b): Experimental results obtained in the Janssen experiment. c): Differential granular media volume indicating its three surfaces: A_1, A_2 and A_s [5, 6]. d): Experimental set-up for the determination of the static friction coefficient

II. THEORETICAL FRAMEWORK

II.1. Revisiting Janssen model

Janssen modeled this behavior by considering the granular media as a continuum material whose stress tensor $\bar{\bar{\sigma}}$ is diagonal with $p = -\sigma_{zz}$ and verifies:

$$k\sigma_{zz} = \sigma_{rr} = \sigma_{\phi\phi}\,, \tag{1}$$

in cylindrical coordinates r, ϕ and z (notice that in the following we differentiate p for the pressure in the medium and P for the pressure measured at the bottom of the medium). In order to account for friction between the granular media and the walls ($r = R$), it is also fulfilled:

$$\sigma_{zr}(R) = \mu_s\sigma_{rr}(R) = \mu_s k\sigma_{zz}\,. \tag{2}$$

Here μ_s is the static friction coefficient and k is the proportionality constant related horizontal and vertical stresses. By considering a cylindrical element of volume with radii R and height dz, , see Fig.1 c), we can consider mechanical equilibrium, including body and contact forces, as encompassed in the stress tensor $\bar{\bar{\sigma}}$:

$$\int_V \overrightarrow{f}\; dV + \oint_S \bar{\bar{\sigma}}\; \cdot \overrightarrow{dS} = 0 \tag{3}$$

by making use of Eq. (1) and Eq. (2), the second term on the LHS can be written as

$$\oint_S \bar{\bar{\sigma}}\; \cdot \overrightarrow{dS} = -\pi R^2\sigma_{zz}(z)\hat{z} + \pi R^2\sigma_{zz}(z+\Delta z)\hat{z} + 2\pi Rk\mu_s\sigma_{zz}\Delta z\hat{z}\,, \tag{4}$$

where z it he depth. The first term in Eq. (3) can be directly written as

$$\int_V \overrightarrow{f}\; dV = \rho g\pi R^2\Delta z\hat{z} \tag{5}$$

Regrouping Eqs. (4) and (5), and taking the continuum limit $\Delta z \to 0$, we obtain the following differential equation:

$$\frac{d\sigma_{zz}}{dz} = -\rho g - \frac{2k\mu_s}{R}\sigma_{zz} \tag{6}$$

Integrating Eq. (6) using the boundary condition $\sigma_{zz}(z = 0) = 0$, and defining $\lambda = R/2k\mu_s$ we get the following expression for the pressure:

$$p(z) = \rho g\lambda(1 - e^{-z/\lambda}) \tag{7}$$

So that, the pressure at the bottom of a column of height h will be

$$P(h) = \rho g\lambda(1 - e^{-h/\lambda})\,. \tag{8}$$

Finally, Eq. (8) can be written in terms of the added mass and the apparent mass ($P(h)\pi D^2/4 = m_{app}g$) defining a saturation mass $M \equiv \rho\pi D^3/16\mu_s k$, where now ρ is the mean density of the granular column and D is the diameter of the container

$$m_{app} = M(1 - e^{m_{add}/M}) \tag{9}$$

This model for the pressure captures the physical origin of the pressure saturation that was observed experimentally for corn. Janssen's experiment is a benchmark for the studies in granular materials and for that reason, it has been reproduced many times. However, it has been largely proved that the mathematical model derived by Janssen [5] does not fit quantitatively with experiments. As explained in [7, 14], the actual experimental data show larger values for $P(h)$ than the predicted one.

II.2. Corrected Janssen's model for narrow columns

It is stated that the assumptions on Janssen's phenomenological model, being (i) the proportionality of the components of the stress tensor and (ii) the friction reaching its Coulomb's limit, are responsible for underestimating the apparent mass in large containers as well as for overestimating it in small containers [7, 8]. The first assumption implies horizontal regions of equal pressure and the second assumption is stated to be protocol-dependent. However, under different protocols there can be a wide variety of configurations for the pressure surfaces, being concave and convex two extreme cases [15]. The shape of the pressure surfaces is directly connected to the force-chain distribution. Force-chains are internal to the granular column, when are concave from below the chain pushes the container down, resulting in a supportive force experienced by the granular column. On the other hand, when force-chains are convex from below the chain pushes the container up, which in this case results in a force that compresses the granular column.

Both cases are stated to be present whenever filling the granular column sequentially, as in the case of this

experimental work. However, the compression due to chain forces is stated to play a major role the smaller the container is, and gradually disappear when increasing the container diameter [14].

The new features observed on the Janssen experiment, are not captured by the original model, demanded a *corrected* model capable of explaining the occurrence of the overshoot pressure, and at the same time, recover the saturation in pressure expected for large containers. To develop a new model, Mahajan et al [14] considered that the frictional force between the wall of the container and a given particle does depend on the load and depth, and propose a piecewise function for the average frictional force $\langle F_w(z)\rangle$ depending on the column height.

For that reason they define the following characteristic heights: (i) h_a as the height at which m_{app} starts overcoming m_{add}, (ii) h^* as the height at which the column shows its maximum positive deviation from m_{add} and (iii) h_d as the height at which m_{app} starts becoming smaller than m_{add}. With these heights in mind, one can characterize the stress exerted by the walls to the particles on the container, which will depend on the considered depth as

$$\tau(z) = \frac{n_c(D)\langle F_w(z)\rangle}{\pi D}\,. \tag{10}$$

In this expression, $n_c(D)$ is the number of contacts per unit length on the cylindrical container, which has been numerically determined for spherical particles and follows [16]

$$n_c(D) = \frac{a\pi}{\sigma}\frac{D}{\sigma}\frac{1}{1+b\sigma/D}\,, \tag{11}$$

where $a \simeq 0.8$ and $b \simeq 0.9$ are fitting parameters to the experimental points for different D. The depth-dependence of the stress is embedded on the value of the average frictional force $\langle F_w(z)\rangle$, which we assume to be at Coulomb's threshold [19], and varies as:

$$\langle F_w(z)\rangle = \begin{cases} \simeq 0\,, & z < h_a \\ F_c < 0\,, & h_a < z < h^* \\ \dfrac{k\pi D p(z)}{n_c(D)}\left(1 - e^{-(z-h^*)/\xi}\right)\,, & z > h^* \end{cases}$$

In the previous expression, ξ is a decay length which for spherical particles of $\sigma = (5.94 \pm 0.02)$ mm is found to be $\xi \simeq 6\sigma$. The value of F_c is assumed to be constant in the original paper [14]. Its negative sign comes from the fact that is a compressive force, which changes as depth increases, where forces become supportive. With the stress already characterized, we can re-express the condition of mechanical equilibrium:

$$\frac{dp}{dz} = \rho g - \frac{4}{D}\tau(z) \tag{12}$$

This model is capable of describing numerically the results obtained for containers with different diameters and capture both the overshoot region and the saturation in pressure of the Janssen effect [14]. Furthermore, it is possible to extract an analytic solution in the regime in which $z > h^*$ that allows us to predict the maximum deviation of the apparent mass m_{app} from the added mass m_{add}:

$$\max\left[\frac{m_{app}}{m_{add}}\right] - 1 = \frac{F_c n_c(D)}{\pi\rho g D^2}\left(1 - \frac{h_a}{h^*}\right) \tag{13}$$

From Eq. (9) and the already defined expression for $n_c(D)$ (see Eq. (11)) we can find a proportionality relation between the maximum deviation and the diameter of the container, if the assumption of F_c being constant still holds:

$$\max\left[\frac{m_{app}}{m_{add}}\right] - 1 \sim \frac{1}{D}$$

This proportionality has been verified both experimentally and numerically for the case of spherical grains [14]. The consistence of this relation also holds for the original Janssen effect, as it predicts that for $D \to \infty$ we get $\max[m_{app}/m_{add}] \simeq 1$, which is consistent with experimental results as for large containers the reverse Janssen effect does not occur. Thus, they found a phenomenological model capable of describing the overshoot region that takes place in narrow cylinders but also to recover the expected behaviour when the diameter of the container is large.

The aim of this work consists on revisiting Janssen's experiment using grains of different geometries, being lentils and mung beans examples of oblate and prolate geometries, and three cylindrical containers of different sizes. The final goal is to observe experimentally if the overshoot in pressure still occurs when using non-spherical particles, and to help clarifying the impact of the geometry of the grains.

III. MATERIALS AND METHODS

III.1. Experimental setup

For the experiments performed in this work we have used three cylindrical glass tubes with different diameters with $D_S = (20.45 \pm 0.05)$ mm, $D_M = (34.10 \pm 0.05)$ mm and $D_L = (49.15 \pm 0.05)$ mm respectively. We use a camera placed in front of the cylinder to determine the height of the granular column with a spatial sensitivity of $\simeq 0.6$ mm/pix (the sensitivity slightly varies in each experiment) and an analytic scale of resolution $\delta m_{app} = 0.01$g to measure the weight of the granular column. The glass cylinder is sustained on top of two wooden pieces in such a way that neither the pieces nor the tube is in contact with the scale. To connect the granular column with the scale we place a cylindrical piston inside the container, see Fig. 2 panel a). To ensure us that the measures of the mass comes just from the granular column, piston's diameter has to be lower than the inner

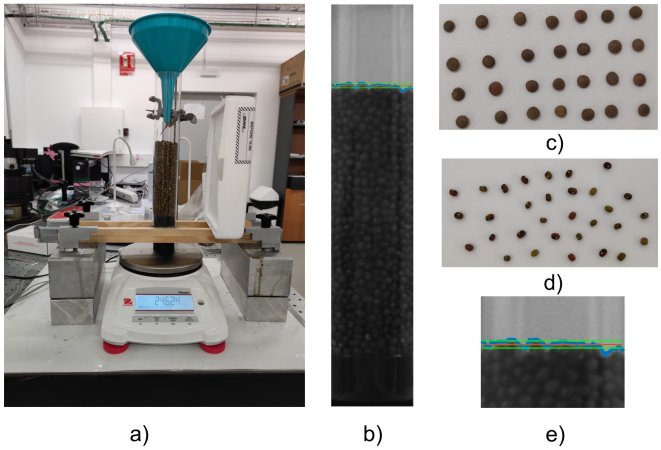

FIG. 2. a): Picture of the experimental set-up using the larger cylinder. b): Example of the determination of the height of the granular column. c): Picture of the oblate grains. d): Picture of the prolate grains. e): Zoom of picture b). The blue line corresponds to the contour of the column. Top green line corresponds to the maximum height of the contour. Bottom green line corresponds to the minimum height of the contour. The red line is the actual determined height, given by the mean height between the two green lines. The error on the height is diven by the standard deviation of this value with respect the maxima and the minima.

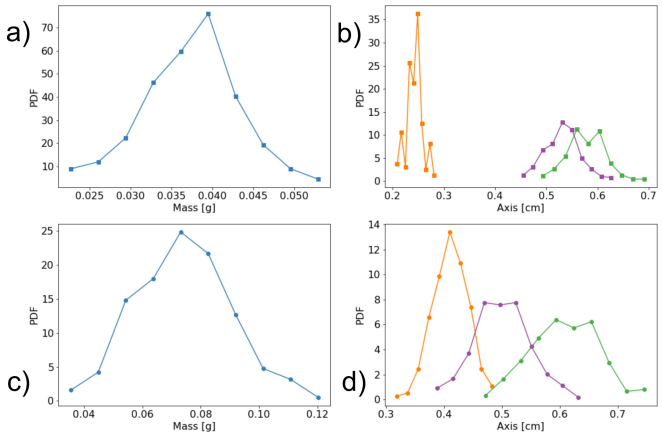

FIG. 3. Statistical results for the measures of 200 particles. Orange represents the thickness of the grain, purple represents the major axis of the grain and green represents the minor axis of the grain. a): PDF for the mass of the oblate particle. b): PDF for the principal axis of the oblate particles. c): PDF for the mass of the prolate particles. d): PDF for the principal axis of the prolate particles

diameter of the container, but large enough so that none of the grains can fall from the column and get trapped between the piston and the container, as in this case the grain would serve as a point of contact and we would be measuring just the total mass of the system. Finally, the whole setup is placed on an optic bench, preventing the system from being perturbed by an external agent such as walking near to the experiment.

III.2. Grains

For the present set of experiments we will use lentils as oblate particles and mung beans as prolate particles, see Fig. 2 c) and d). In order to characterize their masses and sizes, 200 grains were analyzed individually in order to obtain statistics about their mass and characteristic lengths.

Thanks to the values on Fig. 3, we can compute the mean and the standard deviation of the masses, axis and thickness of the particles. From the statistical analysis of the lentils we obtain the mean mass $m_\ell = (37 \pm 6)$ mg, the major and minor axis are $a_\ell = (5.8 \pm 0.4)$ mm and $b_\ell = (5.3 \pm 0.3)$ mm respectively, and the thickness $c_\ell = (2.43 \pm 0.15)$ mm. The results obtained with the beans are $m_b = (74 \pm 16)$ mg, $a_b = (6.1 \pm 0.6)$ mm and $b_b = (5.0 \pm 0.5)$ mm, and $c_b = (4.1 \pm 0.3)$ mm.

Since we are dealing with non-spherical geometries, we have to determine a characteristic diameter if we want to make a similar analysis as for the model proposed on [14]. We define such characteristic diameter as $\sigma = \sqrt[3]{abc}$, so that $\sigma_\ell = (4.2 \pm 0.4)$ mm and $\sigma_b = (5.0 \pm 0.5)$ mm for the lentils and the beans respectively.

Another relevant parameter is the static friction coefficient μ_s between lentils and the containers. The experiment for determining it consisted on joining together five particles and placing the chunk on the container, initially on horizontal position. Fixing the container by one side, we place another cylindrical object below the container, and me make it roll until the chunk of lentils starts moving. Then, we measure the distance between the cylindrical object and the end of the container see, Fig. 1 d). Using this distance and the diameter of the cylindrical container we find the angle θ which is related to the friction coefficient as $\mu_s = \tan(\theta)$. This experiment has been repeated six times for each kind of grain to get a more accurate values. We have obtained $\mu_s^\ell = 0.36 \pm 0.02$ for the lentils and $\mu_s^b = 0.333 \pm 0.007$ for the beans.

III.3. Experimental protocol

Due to the inherent metastability and non-homogeneity of granular media, we end up having systems that are hard to reproduce. This is why protocol plays a key role in experiments concerning grains. Let us consider an example for better understanding this: when filling a container with grains, the state of the system will depend whether grains fall from the center of the container or from one of the sides, which do not happen when filling a container with a liquid. This dependence on the protocol difficulties the task to characterize the system just using the position of the grains, as there are frictional contacts that depend on how the system has been formed. For that reason it is important to describe the experimental protocol when showing experimental results.

In the present set of experiments we add the grains

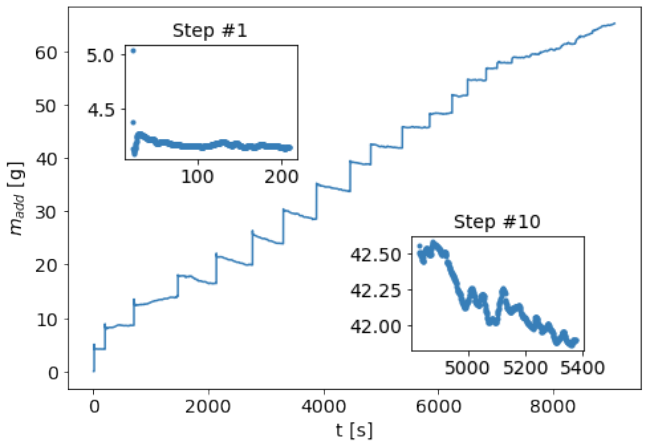

FIG. 4. Experimental data obtained for the apparent mass measured over time for the case of the oblate grains in the medium sized tube. Measures are taken automatically every 0.25 s. The inset plots correspond to zoomed regions corresponding to the first and the tenth layers evolving over time.

using a funnel centered on the container. This way, grains will fall sequentially and approximately from the center of the container. At each measure we will add a fix mass of grains to cover a layer of grains into the container. The mass required for filling one layer at each drop is determined for each combination of column and kind of grain.

Granular matter shows slow dynamics [12].These dynamics also depends on the filling protocol, as experiments that fill the whole column at once at a time show a different relaxation behaviour than when doing it step by step [13]. To perform the experiments we need to establish a characteristic time for our protocol. To do so, I performed experiments for all the grains and containers in which the cylinder was filled layer by layer, letting the system relax for an undetermined amount of time (up to 15 minutes for each layer). From Fig. 4 we notice that looking from a long temporal scale, the behavior of each layer looks very similar. However, when zooming to the actual region we notice that, depending on the step, we find non-monotonic responses of different kinds. Thus, we establish that the criteria for determining the characteristic time τ was to take the initial value of the mass in the step i and the final value of the mass in the same step and compute its difference Δm_{app}. Our characteristic time will then be the time needed to reach the 70% of the absolute variation of added mass along the whole measure $\tau = \ t(m_{app} = 0.7\Delta m_{app}) - t(m_{app,0})$.

III.4. Packing fraction

Thanks to the images captured by a camera (see the set-up in Fig. 2 b)) and using image analysis techniques, we can measure the height of the column at each step, see Fig. 2 e). This allows us to estimate the packing fraction ϕ of the granular column. The packing fraction is defined as the fraction of volume occupied of the actual available volume. To compute this magnitude we consider that particle's irregularities do not play a major role and consider that the geometry of the grains is that of an ellipsoid with volume $V = 4\pi\sigma^3/3$. Thus, we compute the packing fraction of each step as:

$$\phi_i = \frac{N_i \times v_p}{V_i} = \frac{N_i \frac{4\pi}{3}\left(\frac{\sigma}{2}\right)^3}{\pi\left(\frac{D}{2}\right)^2 h_i} = \frac{N_i 2\sigma^3}{3h_i D^2} \qquad (14)$$

where N_i is the mean number of particles at a given step, v_p is the estimated volume of a single grain, V_i is the volume of the granular column at the ith step, and h_i is the corresponding height of the granular column. As we are not counting how many grains we are adding but the mass, we determine this quantity by considering that the mass of each grain is equal to the value of its mean mass $\langle m_\ell \rangle = (37\pm6)$ mg for lentils and $\langle m_b \rangle = (74\pm16)$ mg for the beans, and by knowing the amount of mass added at each step Δm_{added} we determine the number of grains per step as $N_i = \Delta m_{added}/\langle m_{particle} \rangle$ for each combination of grains and tube diameter.

IV. RESULTS

IV.1. Oblate particles

IV.1.1. Large tube

The amount of mass needed to fill one layer at a time of the large tube is $\Delta m_{add} = (8.0\pm0.1)$ g, and the relaxation time of each step is $\tau = 300$ s.

The experiments performed in the large tube, shown in Fig. 5 (TOP), showed a concordance with the model proposed by Janssen for the apparent mass [5]. At the beginning the weight of the column behaves like a fluid but then, around an added mas of 100 g, the apparent mass starts deviating and shows saturation. When comparing with the prediction made by Eq. (9), we notice that the experimental points do follow qualitatively the predicted behaviour but exhibiting slightly larger values on the apparent mass, which is in concordance with previous observations [7, 14]. For that reason, we can make use of the relation $\mathrm{M} = \rho\pi D^3/16\mu_s k$ and adjust it to our data to determine the value of k, see Table I. When performing a different analysis in which we plot the difference between m_{app} and m_{add} to account from the deviation from fluid's hydrostatic pressure Fig. 5 (MIDDLE), a behaviour that is not present in the original Janssen experiment is revealed, as there is a region in which the apparent mass exceeds the added mass, which was observed for the case of spheres [14]. However, our data is noisy in this region so we can not generalize this behaviour for the oblate particles in this tube. The error on the apparent mass was determined as the standard deviation of the measure of 8 g of lentils on the analytic scale during 1000 s

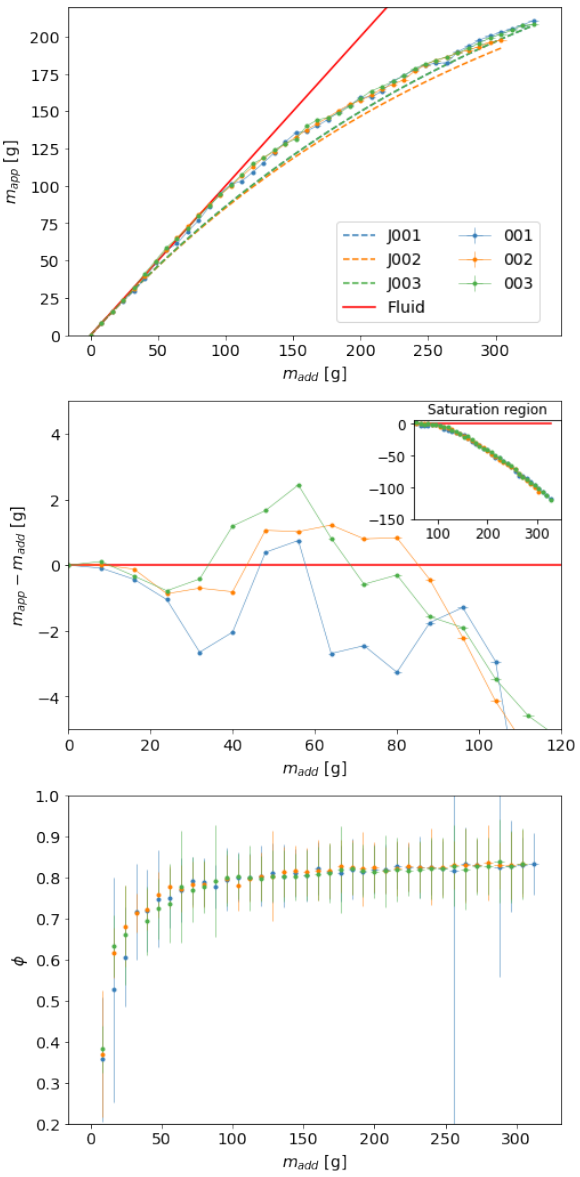

FIG. 5. Results for the Janssen experiment using oblate grains on a cylindrical glass container with diameter D_L. TOP: Results for the m_{app} vs m_{add}. Solid lines represent how a fluid would behave in this experiment. Dashed lines represent fits to the Janssen's model. MIDDLE: Deviation in m_{app} from the added mass as a function of m_{add} represented with points and zoomed on the overshoot region in which the apparent mass is larger than the added mass. The inset plot contains the saturation region, in which the apparent mass is lower than the added mass. BOTTOM: Estimation of the packing fraction of the granular column as a function of m_{add}.

measuring every 0.25 s and is $\delta m_{app} = 0.005\,\mathrm{g}$. The error on the added mass is $\delta m_{add} = 0.1\,\mathrm{g}$ and accumulates on each step. Figure 5 (BOTTOM) shows that the values of the packing fraction increase until $m_{add} \simeq 100\,\mathrm{g}$, which corresponds approximately to the value at which m_{app} starts saturating. After this value of m_{add}, packing fractions fluctuate around a value of $\phi \simeq 0.78$ for all the steps.

Grain geometry	k (Trial 1)	k (Trial 2)	k (Trial 3)
Oblate	3.4 ± 0.2	3.22 ± 0.18	3.40 ± 0.19
Prolate	2.47 ± 0.06	2.73 ± 0.06	2.51 ± 0.06

TABLE I. Values of the estimated proportionality constant between horizontal and vertical stresses k for the different experiments using the large tube with oblate and prolate grain geometries.

IV.1.2. Medium tube

The amount of mass needed for the case of the medium tube is $\Delta m_{add} = (4.0 \pm 0.1)\,\mathrm{g}$ and the relaxation time of each step is $\tau = 210\,\mathrm{s}$.

If we now analyze the results in Fig. 6 (TOP), we observe a similar behaviour as for the case of the large tube, with a saturation of the mass which now shows lower masses than the predicted by Eq. (9) rather than the expected overestimation [7]. This saturation do not seem monotonous, as the apparent mass starts falling and growing when the system enters into the saturation region. When looking at Fig. 6 (MIDDLE) we notice that we begin to see a clear overshoot region in which the apparent mass is larger than the added mass. This behaviour is verified for all trials despite the noise on the data, unlike for the case of the large tube. Due to this behaviour that is not predicted by Eq. (9) we do not estimate the value of k with this tube. Before entering the overshoot region, the system also measures an apparent mass lower than the added mass. To compute the error on the apparent mass we proceeded analogously to the large tube measuring 4 g of lentils on the analytic scale during 1000 s and determined $\delta m_{app} = 0.005\,\mathrm{g}$. As can be observed in Fig. 6 (BOTTOM), the values of the packing fraction increase until $m_{add} \simeq 25\mathrm{g}$, where they fluctuate around $\phi \simeq 0.85$ for all the steps, which is a larger packing than in the large tube case.

IV.1.3. Small tube

The amount of mass needed for the case of the small tube is $\Delta m_{step} = (1.0 \pm 0.1)\,\mathrm{g}$ and the relaxation time of each step is $\tau = 120\mathrm{s}$.

The results for the Janssen experiment on the small tube can be observed in Fig. 7 (TOP), where we recover some similarities with respect the medium tube, as the system deviates from the fluid behaviour and shows a saturation region, which indeed has lower values for the apparent mass than the ones expected from the adjustment to Eq. (9). In this region the granular column do not behave monotonically, as seen for the medium tube, but in this case this behaviour is more amplified.

On Fig. 7 (MIDDLE) we can observe that the overshoot region is present and that is larger and more pronounced than for the case of the medium tube. Another similarity are the initial points in which the apparent mass is lower than the added one, note that this be-

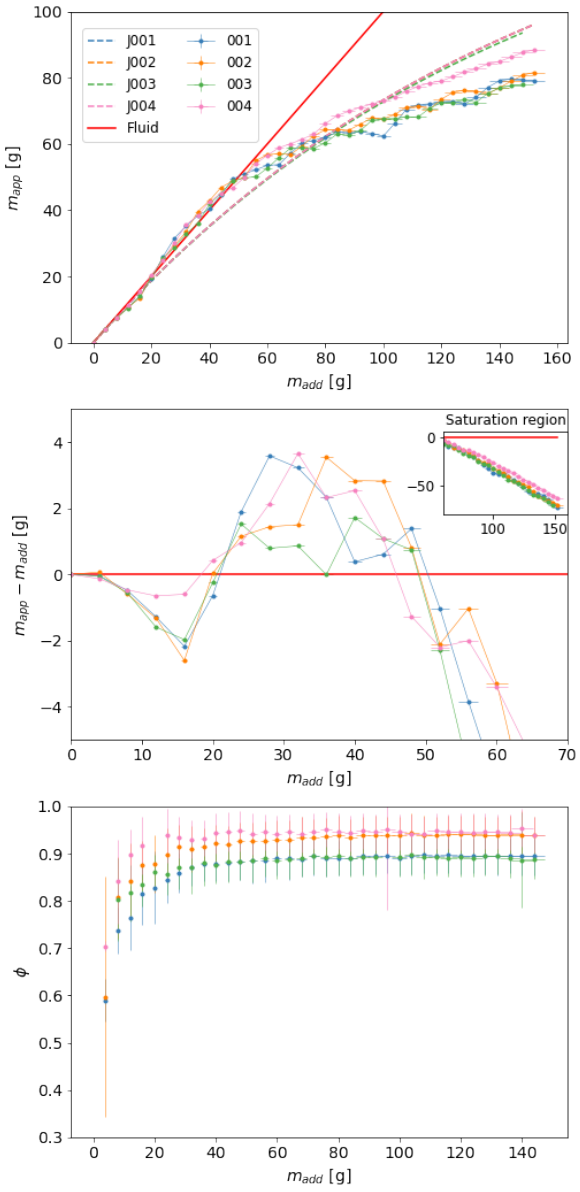

FIG. 6. Results for the Janssen experiment using oblate grains on a cylindrical glass container with diameter D_M. TOP: Results for the m_{app} vs m_{add}. Solid lines represent how a fluid would behave in this experiment. Dashed lines represent fits to the Janssen's model. MIDDLE: Deviation in m_{app} from the added mass as a function of m_{add} represented with points and zoomed on the overshoot region in which the apparent mass is larger than the added mass. The inset plot contains the saturation region, in which the apparent mass is lower than the added mass. BOTTOM: Estimation of the packing fraction of the granular column as a function of m_{add}.

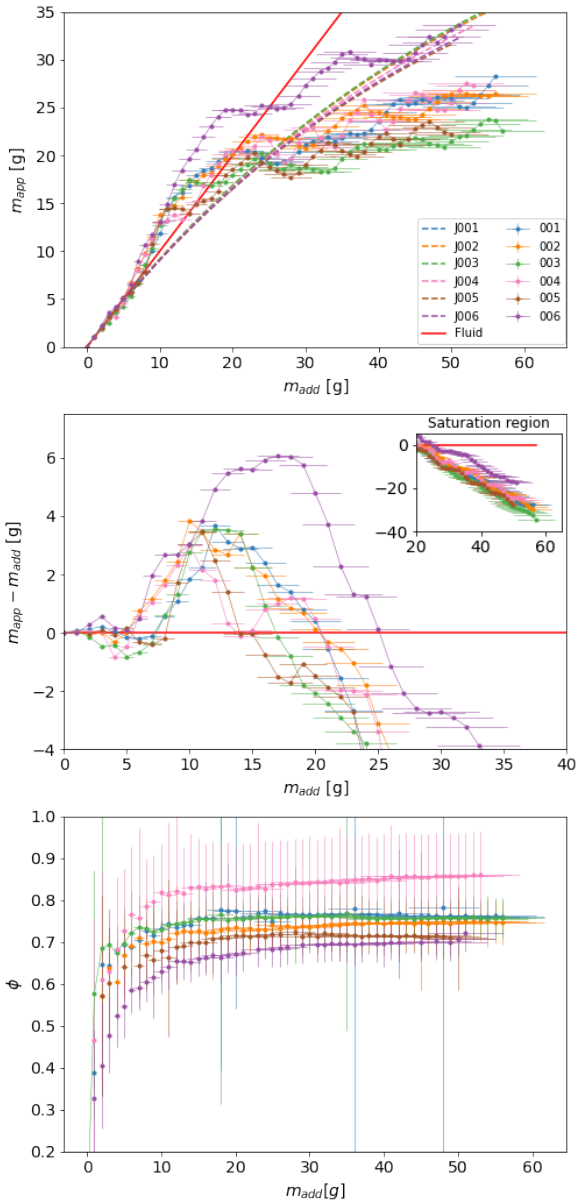

FIG. 7. Results for the Janssen experiment using oblate grains on a cylindrical glass container with diameter D_S. TOP: Results for the m_{app} vs m_{add}. Solid lines represent how a fluid would behave in this experiment. Dashed lines represent fits to the Janssen's model. MIDDLE: Deviation in m_{app} from the added mass as a function of m_{add} represented with points and zoomed on the overshoot region in which the apparent mass is larger than the added mass. The inset plot contains the saturation region, in which the apparent mass is lower than the added mass. BOTTOM: Estimation of the packing fraction of the granular column as a function of m_{add}.

haviour also disappears when entering into the overshoot region. To compute the error on the apparent mass in this case we measured 1 g of lentils on the analytic scale during 1000 s and determined $\delta m_{app} = 0.004\,\mathrm{g}$.

Finally, as can be observed in FIG. 7 (BOTTOM), the values of the packing fraction increase until $m_{add} \simeq 11\mathrm{g}$, where they fluctuate around $\phi \simeq 0.73$ for all the steps, with the exception of experiment 004 whose values are larger, although they also have a larger error.

In Figs. 5, 6 and 7, we can see how does the packing fraction changes with the added mass. These values have been computed considering the mean values of the axis of the oblate grains, so it is indeed an approximated packing fraction. First of all we must rule out all those points

below $\simeq 50\,\%$, typically observed at initial stages. We attribute these low values to the fact that initial layers are more affected by an overestimation of the column's height V_i due to grains that pile-up instead of covering a single layer as we expect. For example, consider the first step: we would be counting two layers instead of one, which is twice as high. However, if we are on the tenth step, then we would be counting eleven layers instead of ten, which is not twice as high.Later drops are less affected by this issue and this effect becomes irrelevant. Apart from that, notice that although we are adding grains without shaking the column, those values do not correspond to the packing fraction of random close packing. This is because friction plays a role in packing, as when we add a new layer we are packing less efficiently than for the case of random packing. The values of the packing fraction saturate at a value $\phi_S \simeq 0.73$, $\phi_M \simeq 0.85$ and $\phi_L \simeq 0.78$ for the small, medium and large tubes respectively. The values for the random close packing of ellipsoids with different aspect ratios ℓ/d where ℓ is the longitudinal axis and d is the diameter of the two-dimensional projection of the ellipsoidal particles $d = \sqrt{ab}$ [17]. For the case of the oblate grains we have an $\ell/d = 0.44$, which allows us to pack randomly with $\phi \simeq 0.71$ [18]. However, we have to remind that we are under presence of gravity so some crystalline regions can arise in the granular columns, which can accommodate larger packing fractions. Thus, the large values of ϕ observed can be explained considering the presence of some crystalline domains along with the values on the error bars.

V. PROLATE PARTICLES

We repeat the experiments now using prolate particles. The amount of mass required for the large tube is $\Delta m_{add} = (6.0 \pm 0.1)\,\mathrm{g}$ and the relaxation time of each step is $\tau = 320\,\mathrm{s}$. The experimental results on Fig. 8 show the same analysis as the one performed for the oblate grains in the large tube. Again, we recover the typical saturation at larger m_{add} observed by Janssen and we see that Janssen's model underestimates the apparent mass. For that reason, we adjust our data to determine the value of k, see Table I. We begin to observe a small overshoot in an intermediate region (see Fig. 8 (MIDDLE)), which is indeed larger and reaches higher values than the experiment performed with oblate grains. The error on the apparent mass has been computed in the same way as for the oblate grains and is $\delta m_{app} = 0.005\,\mathrm{g}$.

Figure 8 (BOTTOM), shows that the values of the packing fraction increase until $m_{add} \simeq 100\,\mathrm{g}$, where they start fluctuating around $\phi \simeq 0.63$ for all the steps, with the exception of experiment 003 whose values are larger and fluctuate around $\phi \simeq 0.69$.

In the case of the medium tube, the amount of mass required for filling one layer with beans is determined as $\Delta m_{add} = (3.0 \pm 0.1)\,\mathrm{g}$ and the relaxation time of each step is chosen to be $\tau = 270\,\mathrm{s}$. Fig. 9 (TOP) shows that, as for the case involving the large tube, Eq. 9 underestimates the value of the apparent mass. This does not happen for what is shown in Fig. 6 (TOP), where in this case it is overestimated. The system does not behave monotonically when entering into the saturation region, as happened for the oblate particles. Fig. 9 (MIDDLE) shows now a clearer overshoot region which is larger and

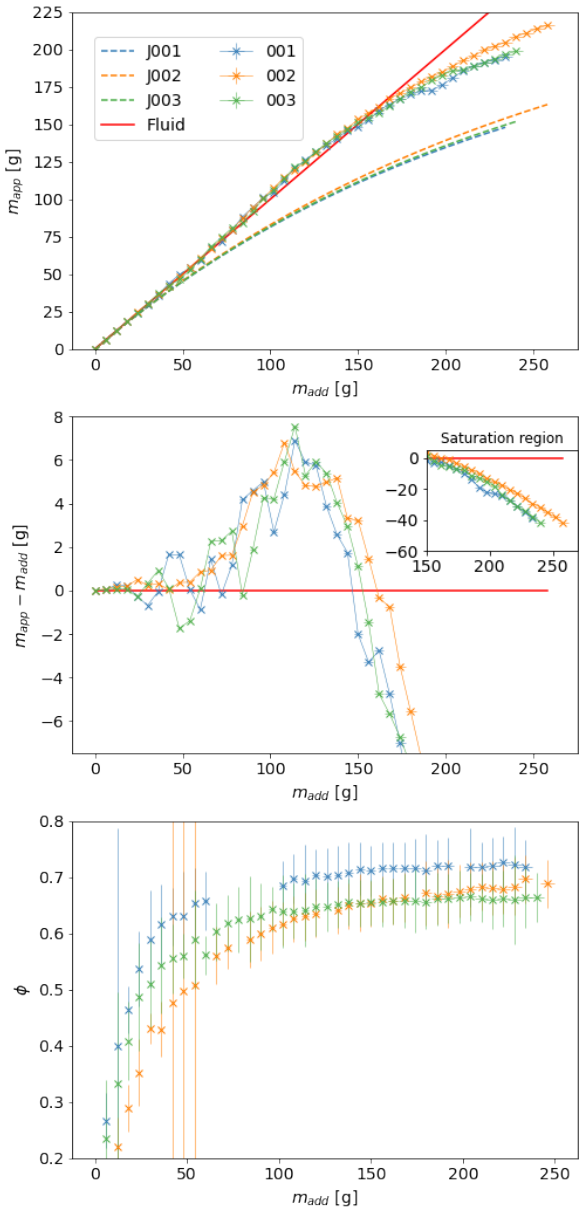

FIG. 8. Results for the Janssen experiment using prolate grains on a cylindrical glass container with diameter D_L. TOP: Results for the m_{app} vs m_{add}. Solid lines represent how a fluid would behave in this experiment. Dashed lines represent fits to the Janssen's model. MIDDLE: Deviation in m_{app} from the added mass as a function of m_{add} represented with points and zoomed on the overshoot region in which the apparent mass is larger than the added mass. The inset plot contains the saturation region, in which the apparent mass is lower than the added mass. BOTTOM: Estimation of the packing fraction of the granular column as a function of m_{add}.

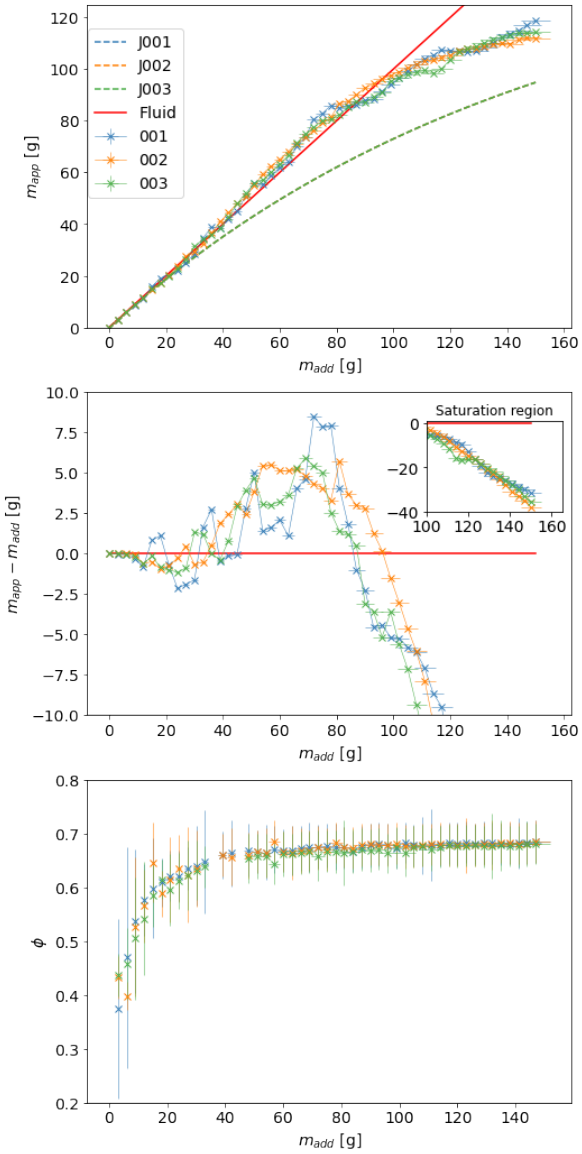

FIG. 9. Results for the Janssen experiment using prolate grains on a cylindrical glass container with diameter D_M. TOP: Results for the m_{app} vs m_{add}. Solid lines represent how a fluid would behave in this experiment. Dashed lines represent fits to the Janssen's model. MIDDLE: Deviation in m_{app} from the added mass as a function of m_{add} represented with points and zoomed on the overshoot region in which the apparent mass is larger than the added mass. The inset plot contains the saturation region, in which the apparent mass is lower than the added mass. BOTTOM: Estimation of the packing fraction of the granular column as a function of m_{add}.

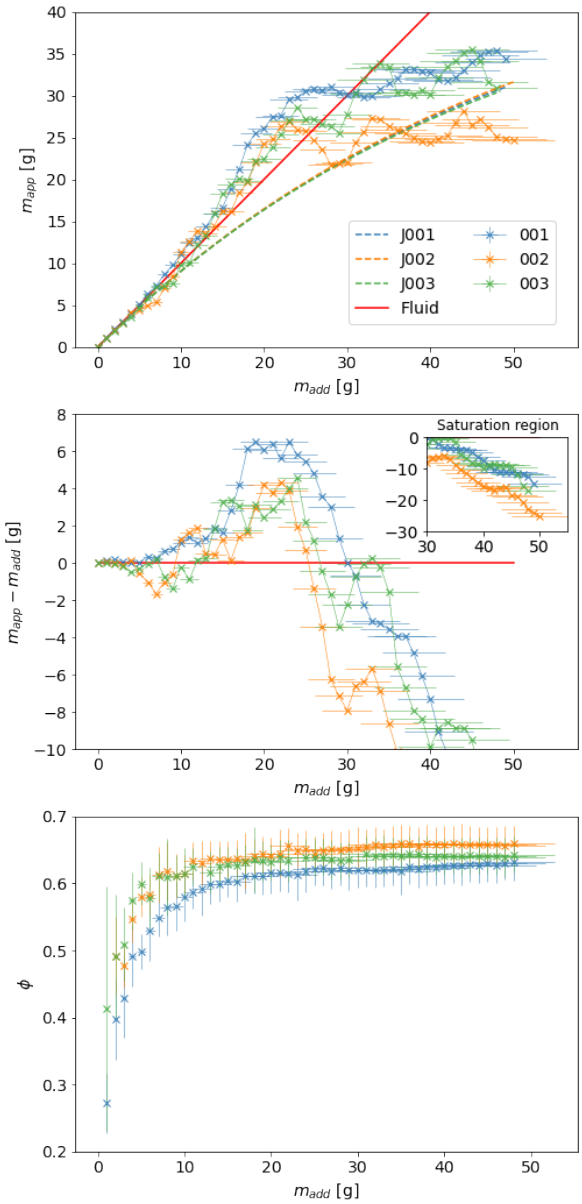

FIG. 10. Results for the Janssen experiment using prolate grains on a cylindrical glass container with diameter D_S. TOP: Results for the m_{app} vs m_{add}. Solid lines represent how a fluid would behave in this experiment. Dashed lines represent fits to the Janssen's model. MIDDLE: Deviation in m_{app} from the added mass as a function of m_{add} represented with points and zoomed on the overshoot region in which the apparent mass is larger than the added mass. The inset plot contains the saturation region, in which the apparent mass is lower than the added mass. BOTTOM: Estimation of the packing fraction of the granular column as a function of m_{add}.

reaches higher values than for the oblate grains using the medium tube. However, when comparing with Fig. 8, one can notice that the region is larger but the values reached do not differ much. This did not happened for the case of oblate geometry. The error on the apparent mass is $\delta m_{app} = 0.005\,\mathrm{g}$. As can be observed in FIG. 9 (BOTTOM), the values of the packing fraction increase until $m_{add} \simeq 40\,\mathrm{g}$, where they start fluctuating around $\phi \simeq 0.65$.

To end up with, we perform experiments using the small cylinder, where the amount of mass required for filling one layer with prolate grains is determined to be $\Delta m_{add} = (1.0 \pm 0.1)\,\mathrm{g}$ and the relaxation time of each step is chosen as $\tau = 180\,\mathrm{s}$.

Fig. 10(TOP) displays a curve with an overshoot re-

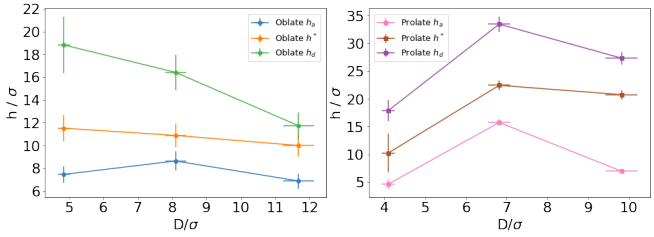

FIG. 11. This figure shows the characteristic heights of oblate (LEFT) and prolate (RIGHT) grains normalized by the mean diameter of the grain and plotted against the diameter of the tube normalized with the mean diameter of the grain.

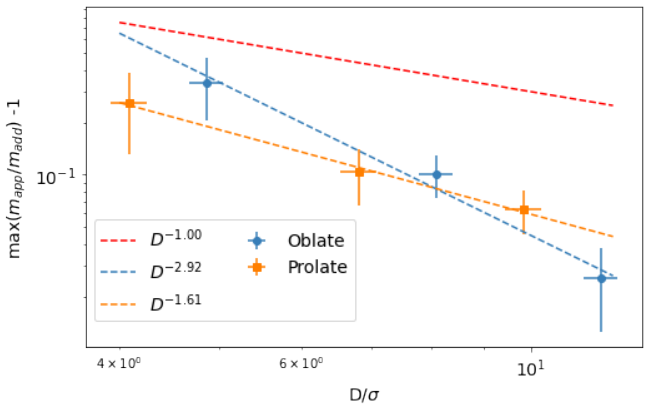

FIG. 12. This figure shows the experimental results for the $\max[\frac{m_{app}}{m_{add}}]$-1 versus the diameter of the tube normalized by the characteristic diameter of the grain in double logarithmic axis. Discontinue lines represents fits to the experimental points, which has been computed using the linear least squares method.

gion and a saturation region, where the values of the apparent mass can be considered to be overestimated by the prediction Eq. 9. The non-monotonous behaviour in this region is clearly observed. Fig. 10(MIDDLE) shows an overshoot region larger than in its analogous with oblate geometry and for the medium and large tubes. Although it reaches higher values than for the oblate grains, those values are similar to the ones observed in Fig. 9 and Fig. 8. The error on the apparent mass is $\delta m_{app} = 0.004\,\mathrm{g}$. As can be observed in FIG. 10 (BOTTOM), the values of the packing fraction increase until $m_{add} \simeq 15\,\mathrm{g}$, where they start fluctuating around $\phi \simeq 0.62$.

When observing the packing fractions for the prolate grains, we must discard all values whose $\phi < 0.5$ as they do not have physical sense, attributing those values to the sensitivity of the first layers to have single grains on a layer above, which results in larger values of V_i. Prolate grains show packing fractions that increase with m_{add} and then fluctuate around $\phi \simeq 0.62$ for the small tube, $\phi \simeq 0.65$ for the medium tube and $\phi \simeq 0.63$ for the large tube. Using the same characterization as for the oblate, we determine a ratio $\ell/r = 1.35$ which allows us to pack randomly with $\phi \simeq 0.68$ [18]. As we are under the presence of gravity, we expect the granular column to have some crystalline domains, that allows larger values on the overall packing fraction so the observed values can accomplished if we also take into account the errors of the magnitude.

VI. DISCUSSION

In order to compare our results with previous experiments performed with spherical particles we will perform the same analysis as in [14],

From the results shown in Fig. 11, we notice that the values of the characteristic heights h_a for the oblate grains are independent of the diameter of the tube D, which is equivalent for the experimental results obtained using spheres [12, 14], while h^* shows a slightly decrease with D. This agreement does not hold for the case of the prolate particles, as we can consider h^* constant for the medium and the large tube, but not for the small tube.We found that for the oblate grains h_d decays with D but it does not saturate as for the spherical particles [14]. However, this is not the case for the prolate ones, where h_d grows with D/σ.

As discussed along section III.4, the phenomenological model described by Janssen [5] is unable to capture the physics of the reverse Janssen effect that takes place when using narrow granular columns [12, 14]. The model proposed in [14] had an analytic solution that allows us to quantify the maximum deviation of m_{app} from m_{add} using Eq. (13). The maximum deviation from from fluid behaviour was experimentally and numerically measured for spheres and agreed to be proportional to D^{-1} [14]. To verify the validity of this model under a change in geometry we perform the same analysis to our data. To do so, each maximum mass has been obtained my taking the mean of the results from the different experiments using the same grain and tube. The error on the maximum mass is the mean of the propagated errors of $m_{app}/m_{add} - 1$ for the different experiments using the same grain and tube. The error on D/σ is obtained with error propagation of D and σ for each grain and tube. From the results shown in Fig. 12, we notice that the change on the geometry has an impact on the maximum deviation from the fluid behaviour, as in the case of spheres it decays as $1/D$, which is not observed neither by the oblate nor the prolate grains, where the decaying is faster in both cases. Despite this non concordance with the model developed for the spheres in [14], we notice that those values are still compatible with a more general power-law behavior $\max[m_{app}/m_{add}] - 1 \sim D^{-\alpha}$. This is in agreement with a similar analysis performed with experiments using garbanzo as a grain [12]. This power-law behaviour is compatible with the expected result for this deviation on the apparent mass in the Janssen effect in non-narrow containers where as $D \to \infty$ the overshoot should disappear, so the value of $\max[m_{app}/m_{add}] - 1$ tends to zero. I summarize in Tab. II the exponents of

Grain geometry	σ (mm)	ℓ/d	α
Spherical [14]	5.94 ± 0.02	1	1.0
Oblate	4.2 ± 0.4	0.44	2.92
Prolate	5.0 ± 0.5	1.35	1.61

TABLE II. Values of the mean diameter σ of the grains, the aspect ratio and the α exponent obtained by fitting a linear regression using least squares to the data shown in Fig. 12.

$\max[m_{app}/m_{add}] - 1 \sim D^{-\alpha}$ fitted for the different grain morphology. The value of those exponents is just an estimation and could be lower if we account for the error bars of the data. Both, oblate and prolate particles, display a decaying power-law behavior as for the case of spherical grains [14]. However, the exponents differ between them. This can be attributed to the fact that the model was developed considering spheres, so the dependence on $n_c(D)$ with D may differ when considering other geometries such as oblate and prolate grains which are known to develop larger coordination [18], which could lead us to obtain larger exponents for D. Notice that for the case of oblate grains, this exponent is much larger than for the prolate. Having larger exponents than for the case of the spheres implies that the *reverse* Janssen effect vanishes at lower values of D when we deviate from the spherical geometry. As the overshoot effect is directly connected with the presence of convex (as seen from below) force chains and both prolate and oblate geometries can have larger packing fractions than spheres [18], there can be a connection between the formation of compressive force chains and the packing of the granular column. Numerical simulations as the performed in [14] using different geometries for the grains could help establishing a connection between packing and force chains.

VI.1. Compaction of the medium

Along section IV and section V we have shown and briefly discussed the values of the packing fractions obtained for the different geometries in the three tubes considered. Although some initial measures had to be discarded, we noticed that the granular media does not have the same packing fraction along all steps, but it rather seems to increase upon reaching a certain value, which could be related with the compaction of the granular column due to gravity effect. To better analyze it, we will show how does the packing fraction vary over the added mass.

From Fig. 13 we observe how the packing fraction vary with the added mass. As for the results of the actual values of the packing fractions, initial points ($m_{add} < 30$g in D_L, $m_{add} < 10$g in D_M, $m_{add} < 5$g for both geometries) do not have to be taken into consideration since they are affected by the experimental resolution. The reason for that is the presence of friction, under which grains can fall on top of other grains and they can remain in that position as they will not slip and fill a hole, which

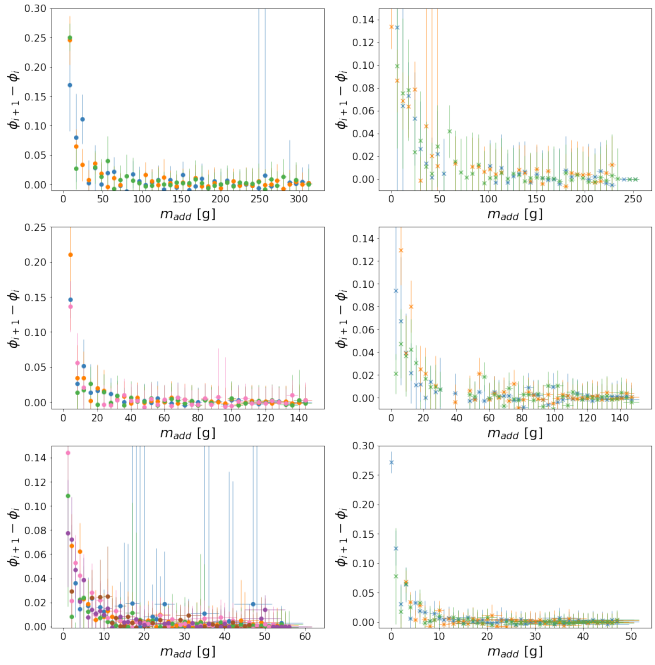

FIG. 13. Variation of the packing fraction between the steps i and $i+1$ plotted against m_{add}. Experimental points using "." correspond to oblate grains. Experimental points using "x" correspond to prolate grains. TOP plots display the results on tube with diameter D_L. MIDDLE plots display the results on tube with diameter D_M. BOTTOM plots display the results on tube with diameter D_S.

makes the system occupy the volume in a less optimized way. This can lead to an overestimation of the height which has more impact on the first drops of grains. For example, let us consider the oblate grains in the small tube. For the first step we have $\phi_1 \simeq 0.39$, corresponding to a height $h_1 = 7.9$mm. If we now consider that we are measuring one layer due to the presence of just a couple of grains, we can subtract $\sigma_\ell/2 = 2.1$mm to the height, as the program computes the value of h_i using the mean height of the contour. Using this new value of the height $h_1' = 5.8$mm we obtain $\phi_1' \simeq 0.53$, which is larger than before and verifies $\phi_1' > 0.5$. Note than even with this correction, the variation of the packing fraction with m_{add} still holds. By using the same argument with step $i = 33$ with $\phi_{33} \simeq 0.77$ we obtain $\phi_{33}' \simeq 0.78$, which means that the previously describe effect has a lower impact the larger the step considered.

We notice that even if we discard those points, the packing fraction differences seem to decrease up to a certain point, where those differences are almost constant. This decaying is in general larger for the lentils than for the case of the beans. One can notice that the added mass at which those differences tend to zero corresponds to the mass right before reaching its maximum value of the overshoot at a column height h^*. The explanation we have for this behaviour is that, as explained in [20], the fact that an sphere has friction allows it to pack loosely. When a grain falls into a layer, in absence of friction, it

will slip and occupy any *hole* in which the grain fits. On the other hand, we are adding more layers at each step, which will interact via body forces with the layers below exerting pressure to them. This pressure compresses the grains of the granular column, thus occupying the volume in a more optimal way. As it has been shown in the experiments for the lentils and the beans, this pressure is related to the apparent mass, and saturates right after reaching h^* due to the Janssen effect. As a consequence, thanks to the friction between the grains and the container that help sustaining the granular column, grains are not compacted anymore due to gravity effects.

VII. CONCLUSIONS

Along this work, Janssen's experiment has been performed using two different grain geometries, being lentils and mung beans, in three tubes with different diameters. Results involving the large tube recover the Janssen effect in which the value of the apparent mass saturates. In both cases it is also common the underestimation of the apparent mass provided by the phenomenological model described in the original work [5], which experimentally appears to be larger for the prolate grains. When decreasing the diameter of the container, a new region where the apparent mass is larger than the added mass appears for both grains geometries. This was not noticed by Janssen [5], but observed in [14]. The responsible to the apparition of this region is argued to be the existence of convex (from below) chain forces that compresses the grains against the scale, allowing the granular column to reach masses larger than the actual mass contained in the cylinder. Although those chains are always present, they play a major role as the size of the tube decreases, which is in concordance with the results obtained for oblate and prolate particles. There are two main differences between the results for the two geometries. The first is the overestimation of the apparent mass from Janssen's model on the oblate grains, which contrasts with the underestimation of the same model when applied to prolate grains. The second is the width and height of the overshoot, which varies more between each tube for the lentils than for the case of the beans.

When comparing those results with the experiments performed with spherical grains filling narrow cylinders we notice some differences. The first is that h_a does not vary when changing the diameter of the tube for the oblate geometry, while h^* shows a slow decaying with increasing D. This does not hold for the case of the prolate geometry, where the value of h^* is the only one that does not vary. Furthermore, the value of h_d is not constant and appears to decrease with the increasing size of the tube for the oblate grains and to increase for prolate grains. On the other hand, the analytical solution of the model developed in [14] proposed a dependence of D^{-1} of the maximum deviation from the fluid behaviour. This is stated to be true for the spheres but not for the oblate nor prolate grains, where this deviation decays faster than what is predicted from the model. The values adjusted from experimental data are $D^{-2.92}$ and $D^{-1.61}$ respectively, although the actual values could be lower considering the error bars.

We have showed that the difference in ϕ goes to zero as we add larger amounts of mass for all the different experiments. The pressure saturates approximately right before h^*, where the differences in packing also become approximately zero. This reinforces the idea that gravity compacts the granular column up to saturation, whereby frictional forces with the walls take over, preventing gravitational forces from further compressing the column irrespective of its height.

Along this work several experimental differences with respect the actual models of Janssen's experiment have been shown. As the characteristic size of both prolate and oblate grains are comparable to the beads used[14] and as the friction coefficient of the grains used in this work are also comparable, differences can be attributed to a change in the geometry and how it affects the packing of the grains.

ACKNOWLEDGMENTS

I would like to thank all the group for the help and support, especially Caleb, whose previous work on the field has allowed me to obtain better quality data. Also thank Ramon and Alberto for the opportunity of working and being part of the group.

[1] P.G. de Gennes, "Granular Matter: A Tentative View," *Reviews of Modern Physics*, vol. 71, no. 2, pp. 374-382, 1999.

[2] H.M. Jaeger and S.R. Nagel, "Granular solids, liquids, and gases," *Review Modern Physics*, vol. 68, no. 4, pp. 1259-1273, 1996.

[3] RP Behringer and B. Chakraborty, "The physics of jamming for granular materials: a review," *Reports on Progress in Physics*, vol. 82, no. 1, pp. 012601, 2019.

[4] M. Cates, J. Wittmer, J.-Ph. Bouchaud and P. Claudin, "Jamming, Force Chains and Fragile Matter," *Physical Review Letters*, vol. 81, no. 9, pp. 1841-1844, 1998.

[5] H. A. Janssen, Z. Verein Deutsch. Ing. vol. 39, pp. 1045, 1895.

[6] M. Sperl, "Experiments on corn pressure in silo cells – translation and comment of Janssen's paper from 1895," *Granular Matter*, vol. 8, pp. 59–65, 2006.

[7] L. Vanel, Ph. Claudin, J.-Ph. Bouchaud, M. E. Cates, E. Clément and J. P. Wittmer, "Stresses in Silos: Comparison Between Theoretical Models and New Experiments," *Physical Review Letters*, vol. 84, no. 7, pp. 1439-1442, 2000.

[8] I. Bratberg, K. J. Måløy and A. Hansen, "Validity of the Janssen law in narrow granular columns," *The European Physical Journal E*, vol. 18, no. 3, pp. 245-252, 2005.

[9] Y. Bertho, F. Giorgiutti-Dauphiné and J.-Pi. Hulin, "Dynamical Janssen Effect on Granular Packing with Moving Walls," *Physical Review Letters*, vol. 90, no. 14, pp. 144-301, 2003.

[10] R. Chand, M. A. Khaskheli, A. Qadir, Y. Sandali and Q. Shi, "Influence of spontaneous percolation on apparent mass at the bottom of a Janssen granular column," *Physica A: Statistical Mechanics and its Applications*, vol. 393, no. C, pp. 96-100, 2014.

[11] T. Bertrand, R. P. Behringer, B. Chakraborty, M. D. Shattuck and C. S. O'Hern, "Protocol dependence of the jamming transition," *American Physical Society (APS)*, vol. 93, no. 1, pp. 12-901, 2016.

[12] C. J. Anderson, "Clusters, waves, and force chains in fire-ant collectives: Emergent behaviour in out-of-equilibrium particulate systems," Dissertation, Georgia Institute of Technology, GA, 2021.

[13] A. Qadir, Z. H. Memon and F. Shah, "Validity of the Janssen Model for Layered Structures in a Silo," *Mehran University Research Journal or Engineering and Technology*, vol. 30, no. 3, pp. 405–410, 2011.

[14] S. Mahajan, M. Tennenbaum, S. N. Pathak, D. Baxter, X. Fan, P. Padilla, C. Anderson, A. F. Nieves and M. P. Ciamarra, "Reverse Janssen Effect in Narrow Granular Columns," *Physical Review Letters*, vol. 124, no. 12, pp. 128002, 2020.

[15] J. H. Shaxby, J. C. Evans and V. Jones, "On the properties of powders. The variation of pressure with depth in columns of powders," *Transactions of the Faraday Society*, vol. 19, pp. 60-72, 1923.

[16] S. Mahajan, M. Tennenbaum, S. N. Pathak, D. Baxter, X. Fan, P. Padilla, C. Anderson, A. F. Nieves and M. P. Ciamarra, "Supplemental Material for "Anomalous Janssen Effect In Narrow Granular Columns," *Physical Review Letters*, vol. 124, no. 12, pp. 128002, 2020.

[17] T. Börzsönyi and R. Stannarius, "Granular materials composed of shape-anisotropic grains," *Soft Matter*, vol. 9, no. 31, pp. 7401-7418, 2013.

[18] A. Donev, I. Cisse, D. Sachs, E. A. Variano, F. H. Stillinger, R. Connelly, S. Torquato and P. M. Chaikin, "Improving the density of jammed disordered packings using ellipsoids," *Science (New York, N.Y.)*, vol. 303, pp. 990-993, 2004.

[19] C. Coulomb, "In Memoir de Mathematique et de Physique," *Academie des Sciences, L'Imprimerie Royale*, vol. 7, pp. 343, 1773.

[20] G. R. Farrell, K. M. Martini and N. Menon, "Loose packings of frictional spheres," *Soft Matter*, vol. 6, no. 13, pp. 2925-2930, 2010.